QUANTUM COMPUTING

High-fidelity teleportation of a logical qubit using transversal gates and lattice surgery

C. Ryan-Anderson*, N. C. Brown, C. H. Baldwin, J. M. Dreiling, C. Foltz, J. P. Gaebler, T. M. Gatterman, N. Hewitt, C. Holliman, C. V. Horst, J. Johansen, D. Lucchetti, T. Mengle, M. Matheny, Y. Matsuoka, K. Mayer, M. Mills, S. A. Moses, B. Neyenhuis, J. Pino, P. Siegfried, R. P. Stutz, J. Walker, D. Hayes

Quantum state teleportation is commonly used in designs for large-scale quantum computers. Using Quantinuum's H2 trapped-ion quantum processor, we demonstrate fault-tolerant state teleportation circuits for a quantum error correction code—specifically the Steane code. The circuits use up to 30 qubits at the physical level and employ real-time quantum error correction. We conducted experiments on several variations of logical teleportation circuits using both transversal gates and lattice surgery. We measured the logical process fidelity to be 0.975 ± 0.002 for the transversal teleportation implementation and 0.851 ± 0.009 for the lattice surgery teleportation implementation as well as 0.989 ± 0.002 for an implementation of Knill-style quantum error correction.

The quantum teleportation protocol, discovered by Bennett *et al.* (*1*) and demonstrated soon after (*2*–*6*), allows a qubit to be teleported between two registers by predistributing an entangled qubit pair and transferring two bits of classical information. This protocol is vital for quantum computing and networks, enabling qubit interactions in nonlocal geometries where moving qubits is difficult. By distributing entangled pairs across a quantum computer, qubits can be transmitted as quickly as classical information. As fault tolerance is essential for large quantum computations, logical teleportation becomes truly enabling (*7*, *8*).

Here, we demonstrate the maturity of H-series trapped-ion quantum processors by performing the first fault-tolerant state teleportation circuit using a quantum error correction (QEC) code with a distance of three or greater. Four logical teleportation variants, using up to 30 trapped-ion qubits and real-time QEC, are contrasted with physical qubit teleportation. Two logical variants use lattice surgery to implement logical gates, including an early demonstration of lattice surgery on QEC codes. These experiments used Quantinuum's H2 trapped-ion quantum processor with 32 physical qubits (*9*). More hardware details are provided in the text and the supplementary materials (SM).

Experimental designs

The goal of teleportation is to transfer a state $|\psi\rangle$ from one qubit to another qubit using entangled resources without entangling the initial and final qubits. We refer to the input qubit as qubit one and the resources as qubits two and three. First, qubits two and three are entangled into a Bell pair, $(|00\rangle + |11\rangle)/\sqrt{2}$. A joint $X \otimes X$ measurement of qubits one and two is performed. Qubit three is then measured in the Z basis, which equivalently measures $Z \otimes Z$ between qubits two and three. These two measurements yield two bits of classical information, which reveals global bit and phase parities and is used to apply single-qubit operations on qubit three. This effectively transfers $|\psi\rangle_L$ to qubit three, thus completing the teleportation.

The sections that follow describe the three distinct groups of teleportation experiments we performed: (i) a physical-level protocol, (ii) a logical-level protocol using transversal gates, and (iii) a logical-level protocol using lattice surgery gates.

Physical-level experiment

A performance baseline was established by characterizing the teleportation protocol at the physical level, that is, without encoding (see Figs. 1 and 2). To average across the four zones in the H2 (*9*) device that perform both gating and measurement, we ran four independent teleportation circuits in parallel, using 12 qubits.

The teleportation circuit was benchmarked by sending an informationally complete set of states through the circuit and measuring the probability of finding the correct state at the output. The six eigenstates of the single-qubit Pauli operators were used as inputs: $\psi \in \{|0\rangle, |1\rangle, |+\rangle, |-\rangle, |+i\rangle, |-i\rangle\}$. The average state fidelity of the teleportation over this set is $F_a = \frac{1}{6}\sum_\psi p_\psi$, where p_ψ is the probability of finding the correct state as the output. This quantity determines the process fidelity using $F_p = [(d+1)F_a - 1]/d$ (*10*), where the dimension is $d = 2$ for teleportation of a single qubit. This method of fidelity estimation does not distinguish different sources of error (e.g., state preparation and measurement errors versus gate and memory errors). In this work, we focused on the different teleportation protocols studied and their overall fidelity instead of component-level analysis (*11*).

We measured the process fidelity of the physical-level teleportation to be 0.9895 ± 3 (details in Fig. 1, Table 1, and table S1). We note that the state fidelities of the physical-level experiment are lower for the −1 eigenstates compared with the +1 states, possibly because of a known bias at the physical level in measuring $|0\rangle_L$ with slightly higher fidelity than $|1\rangle_L$ (*12*) (see Discussion and SM supplementary text section 4 for bias noise discussions).

Logical-level experiments: Transversal circuits

In this section, we describe experiments using transversal operations. In benchmarking transversal logical operations and fault-tolerant logical circuits, measuring syndromes and determining corrections is crucial. To ensure fault tolerance, we included "QEC gadgets" in our experiments. Unlike general rounds of syndrome extraction, a QEC gadget is a discrete

Table 1. The measured fidelities of teleportation protocols. All six eigenstates of the three Pauli operators were used as inputs, with each state's fidelity denoted as F_S. The informationally complete set of states is sufficient to estimate the average state fidelity F_a and process fidelity F_p.

$\|\psi\rangle$	Physical	0QEC	1QEC	$M_{XX}M_{ZZ}$	M_{ZZ}
$\|0\rangle$	0.9949^{+2}_{-2}	0.999^{+1}_{-1}	0.990^{+2}_{-2}	0.950^{+4}_{-4}	0.957^{+3}_{-3}
$\|1\rangle$	0.9932^{+3}_{-3}	0.9987^{+9}_{-9}	0.988^{+4}_{-4}	0.943^{+7}_{-7}	0.953^{+6}_{-6}
$\|+\rangle$	0.9941^{+8}_{-8}	0.991^{+2}_{-2}	0.983^{+3}_{-3}	0.88^{+1}_{-1}	0.925^{+8}_{-8}
$\|-\rangle$	0.9928^{+3}_{-3}	0.990^{+3}_{-3}	0.983^{+4}_{-4}	0.91^{+2}_{-2}	0.93^{+1}_{-1}
$\|+i\rangle$	0.9923^{+3}_{-3}	0.991^{+2}_{-2}	0.975^{+4}_{-4}	0.87^{+2}_{-2}	0.90^{+2}_{-2}
$\|-i\rangle$	0.9907^{+3}_{-3}	0.985^{+4}_{-4}	0.983^{+5}_{-5}	0.86^{+2}_{-2}	0.88^{+2}_{-2}
F_a	0.9930^{+2}_{-2}	0.992^{+1}_{-1}	0.984^{+1}_{-1}	0.901^{+6}_{-6}	0.925^{+5}_{-5}
F_p	0.9895^{+3}_{-3}	0.989^{+2}_{-2}	0.975^{+2}_{-2}	0.851^{+9}_{-9}	0.887^{+7}_{-7}

Quantinuum, Broomfield, CO 80021, USA.
*Corresponding author. Email: ciaran.ryan-anderson@quantinuum.com

circuit dedicated to the collection of syndrome measurement to fault-tolerantly determine a correction, analogous to the error correction gadgets in extended rectangle formalism (*13*). This approach differs from spacetime codes (*14*), where syndrome extraction is spread throughout the logical circuit, and decoding may cover a larger section of the circuit.

The circuit is encoded with the Steane code (*15*), which has been used in many demonstrations of logically encoded circuits (*8*, *16*–*18*), including our work (*11*, *19*–*21*). For this Steane code implementation, a fault-tolerant QEC gadget uses up to two rounds of syndrome extraction, with the second round being executed upon detecting a syndrome change. Our previous work (*19*) showed that 80% of the time, only one round was needed. Since that work, error rates in our devices have been reduced, and it is likely that for the experiments in this work, >80% of the time, each QEC gadget runs only one round of syndrome extraction. Such adaptive syndrome extraction methods allow one to only measure the syndromes that are needed for fault tolerance and avoid injecting unnecessary circuit noise (*19*, *22*).

We included QEC gadgets in some of these circuits, but, to help characterize the logical error budget, we also examined circuits without QEC gadgets. The teleportation circuit using transversal CNOTs (controlled NOT gates) is illustrated in Fig. 3. All the techniques and subroutines relevant to this section are detailed in (*19*, *20*), and here we provide a brief overview of them.

The logical-level teleportation circuit mirrors the physical-level one but includes circuitry needed for encoding and QEC. Logical qubits two and three are prepared in 0_L using a fault-tolerant encoding circuit, including a nondestructive logical $\bar{Z}$ measurement, followed by transversal Hadamard and CNOT gates to create the Bell pair. Both qubits then undergo flagged syndrome extraction (*19*), measuring six syndromes each. These extraction circuits are part of the resource Bell-state preparation, all occurring before these qubits interact with $|\psi\rangle_L$ (Fig. 3).

We take advantage of the resource state construction by noting that, in large-scale fault-tolerant architectures, it is scalable to use postselection to create resource states such as magic states or Bell pairs. Such architectures assume that large devices can prepare resource states in parallel, ensuring availability when needed (*23*–*27*). In this work, Bell states were postselected using verification measurements in the encoding circuit and syndrome measurements after entangling operations. Following Goto's fault-tolerant logical zero initialization scheme (*28*), each logical qubit of the Bell pair was prepared in logical zero, verified, and postselected if any logical zero preparations failed. After applying transversal logical Hadamard and CNOT gates to entangle and prepare the logical Bell state, we measured six independent weight-four stabilizers of the Steane code and postselected if any syndromes were nontrivial. This scheme does not eliminate all errors; for example, weight-three faults resulting in a logical operator being applied would go undetected.

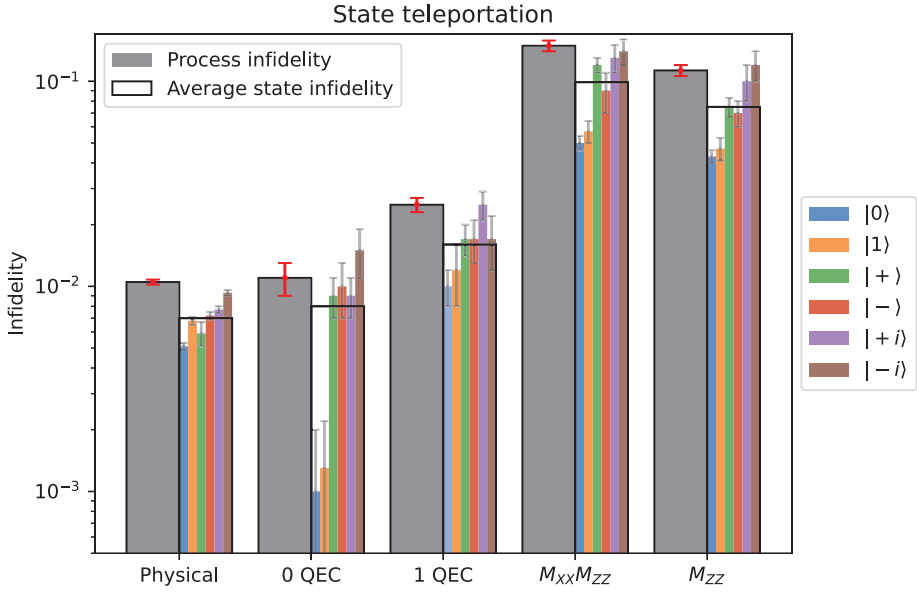

Fig. 1. The measured infidelities of teleportation protocols. All six eigenstates of the three Pauli operators were used as inputs, with each state's infidelity denoted by a different color. The informationally complete set of states is sufficient to estimate the average state infidelity $1 - F_a$ (clear box around individual infidelities) and process infidelity $1 - F_p$ (gray box).

Fig. 2. The general circuit for the teleportation circuit. The highlighted subcircuit labeled "Bell state prep." creates the entangled Bell pair $(|00\rangle + |11\rangle)/\sqrt{2}$.

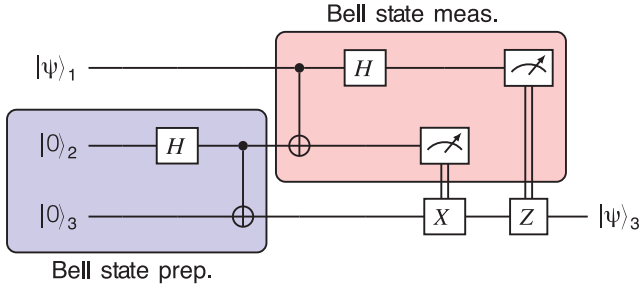

After the Bell state was prepared, logical qubit one was initialized to $|0\rangle_L$ using the encoding circuit (*19*, *28*). In contrast to the preparation of the Bell-state resource, the encoding circuit for logical qubit one uses up to three rounds of a repeat-until-success (RUS) protocol (*19*), at which point the circuit proceeds regardless of the outcome of the verification step. That is, we did not postselect on the preparation of logical qubit one. After preparing $|0\rangle_L$, a transversal single-qubit Clifford operation, natively admitted by the Steane code, can prepare one of the six states, $\{|0_L\rangle, |1_L\rangle, |+_L\rangle, |-_L\rangle, |+i_L\rangle, |-i_L\rangle\}$. Further description of the postprocessing procedure and detailed data on the number of shots discarded are provided in SM supplementary text section 3.

We implemented two variants of the logical circuit depicted in Fig. 3, which differ only by the presence of a full QEC gadget on logical qubit one. Given the importance of QEC gadgets in large-scale fault-tolerant computation, we considered benchmarking with the QEC gadget included as important. However, examining the circuit without the QEC gadget offered insight into the logical error contributions of the teleportation protocol. We refer to the protocol that includes one QEC gadget on logical qubit one as "1QEC" and the protocol without the QEC gadget as "0QEC." Notably, the entire 0QEC experiment can be viewed as the implementation of a QEC gadget as originally proposed by Knill (*26*, *29*). See SM supplementary text section 5 for details.

In the 1QEC experiment, the QEC gadget was the full conditional adaptive syndrome extraction described in (*19*). The extracted syndromes were processed in real time using a look-up table decoder. Active error correction was then applied by physically applying Pauli corrections (instead of Pauli frame tracking).

Next, we performed the Bell measurement on logical qubits one and two by destructively

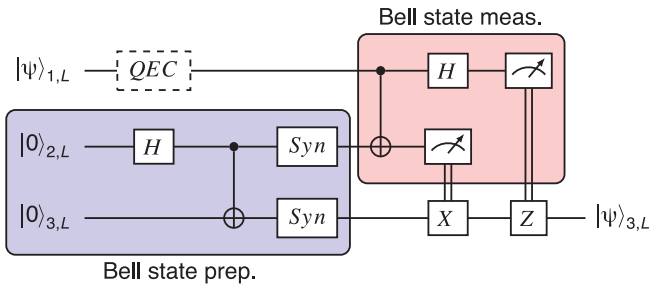

Fig. 3. The logical-level circuit for the teleportation circuit. The gadget labeled "QEC" is a full QEC round with up to two rounds of adaptive syndrome extraction (*19*, *22*), and the box is dashed to highlight that it is omitted in some experiments. The subcircuit labeled "Bell state prep." shows where the entangled Bell pair is created, which we consider a resource state. The gadgets labeled "Syn" are each a round of flagged syndrome extraction used to postselect Bell-state preparations without nontrivial syndrome measurements.

measuring all of their data qubits. The measurements were used to reconstruct syndrome information and decode and correct the logical outcomes. The corrected outcomes were then used to update the Pauli frame of qubit three, in a manner equivalent to conditionally applying the classically controlled Pauli gates on qubit three.

To measure the probability of finding the correct state in logical qubit three (i.e., determine the state fidelity), we applied a single-qubit transversal gate to measure in a particular basis, destructively measure all data qubits, reconstruct syndromes, decode, and apply corrections to the final logical outcome [see (*19*) for details].

Real-time decoding occurred four times in this circuit. During the QEC gadget and the three destructive logical measurements, the decoder processed syndromes and determined corrections.

We estimated the process fidelities for 0QEC (or, equivalently, Knill QEC) to be 0.989 ± 1 and for 1QEC to be 0.975 ± 2. This suggests that the QEC gadget is one of the noisier components of the circuit, consistent with previous measurements (*19*, *20*). There was also a difference in the total number of physical qubits used in each experiment, with the 1QEC version using 30 physical qubits (10 for each code block) and the 0QEC gadget using 28 (10 for each code block in the Bell state, and for the other code block, seven data qubits and an additional verification ancilla).

Logical experiment: Lattice surgery

Transversal operations are not the only methods for performing logical gates. We demonstrate the flexibility of the quantum charge-coupled device (QCCD) architecture (*30*) by looking at equivalent teleportation circuits built from a Steane code lattice-surgery gate set (*31*). Lattice surgery uses two-dimensional (2D) nearest-neighbor interactions, making it ideal for fixed 2D qubit architectures (*31*, *32*). This method involves measuring joint logical Pauli operators when merging code blocks. We extended these techniques—which were previously demonstrated in ion traps with $d = 2$ surface codes (*7*)—to the $d = 3$ Steane code.

An analogous logical teleportation circuit using lattice surgery is shown in Fig. 4. Some methods used here are identical to those used in the transversal circuits, such as the initialization protocols of all three logical qubits, transversal Hadamard gates, decoding, and destructive measurements.

The Bell-state preparation uses lattice-surgery gate sets. After qubits two and three have been initialized, a joint $\overline{X_2X_3}$ logical operator is measured (fig. S4). This measurement scheme includes an additional physical flag qubit to catch higher-weight hook errors (*19*, *33*, *34*). After the measurement of the joint logical operator, we performed one round of syndrome extraction using flagged checks (also used in the "Syn" gate in Fig. 3). We again treated the Bell state as a resource state and postselected on the same criteria as the transversal implementation (encoding verification failing and any nontrivial syndromes) and any nontrivial measurement from the flag qubit in the $\overline{X_2X_3}$ joint logical measurement. For this experiment, we only postselected on the Bell-state preparation. We decoded the syndrome information in real time, using the same decoder as in the other experiments, and kept track of corrections on qubit three by means of a Pauli frame.

The circuit proceeded by measuring a second joint logical operator $\overline{Z_1Z_2}$, again using a flag circuit (fig. S5). We then performed a full QEC gadget with both the flagged and conditional unflagged syndrome measurements. If the logical measurement flag or any syndromes in the QEC gadget were nontrivial, we repeated the measurement of $\overline{Z_1Z_2}$, followed by the "Syn" gadget syndrome measurements (Fig. 3). We treated this second measurement round as ideal and continued. If the first round of measurements of $\overline{Z_1Z_2}$ and the full QEC gadget yielded trivial flags and syndromes, the second round of measurements was skipped. The rest of the circuit involved transversal Hadamard gates, destructive measurements, decoding, and conditional corrections tracked by means of a Pauli frame, all of which were handled in the same way as in the transversal teleportation circuits. A total of 30 physical qubits were used in this experiment: 10 qubits for each individual code block. The lattice-surgery circuit, which we call $M_{XX}M_{ZZ}$, was measured to have a process fidelity of 0.851 ± 9. For further analysis on viewing these results as QED codes, see SM supplementary text section 2.

Lattice surgery offers more than an alternative way to implement logical gates; it can also reduce overheads in some cases (*35*). We investigated a logical teleportation circuit using two logical qubits instead of three, which does not use a Bell-state resource but is algorithmically equivalent to the teleportation protocol. A proof of this equivalency is provided in the supplementary materials (fig. S1). This form of lattice surgery teleportation involves merging a logical qubit with an ancillary code block and then shrinking it back to transfer the logical state. This technique, akin to one-bit teleportation (*36*), can be used for code-switching and gate teleportation (*37*). Previously implemented for a $d = 2$ QED code (*7*), we applied it here to a QEC code with real-time decoding and error correction.

The simpler teleportation circuit can be seen in Fig. 4B. The beginning of the circuit was similar to the other experiments, using encoding circuits with verification ancilla implemented in a RUS protocol to encode $|0_L\rangle$. The RUS circuit was performed up to three times for both logical qubits to achieve high-fidelity input states. Next, the joint Pauli $\overline{Z_1Z_2}$ logical operator was measured, followed by a full QEC gadget. The rest of the circuit, including decoding, correction tracking by means of a Pauli frame, transversal single-qubit gates, and destructive measure-outs, was performed like all the other experiments.

We measured this lattice surgery circuit, which we call M_{ZZ}, to have a process fidelity of 0.887 ± 7. Only 20 qubits were needed in this implementation, 10 for each individual code block, and a maximum of 136 physical CNOTs were required. Further details are given in Fig. 1 and SM supplementary text section 2.

Discussion

The results of all the experiments are presented in Fig. 1 and Table 1 (see SM supplementary text sections 2 to 4 for additional details). One feature of the data reflects the asymmetric memory error of the H-series quantum computers, which is likely dominated by stochastic and coherent rotations about Z. As noted in (*19*), because the logical $\bar{Z}$ operator is a product of Zs, we find a higher probability of logical Z errors [see figure 1 in (*19*)]; therefore, $\bar{X}$ and $\bar{Y}$ basis states have lower fidelity. Physical layer fidelities do not show this asymmetry because they are not dominated by memory error. [See (*12*) for noise model details.]

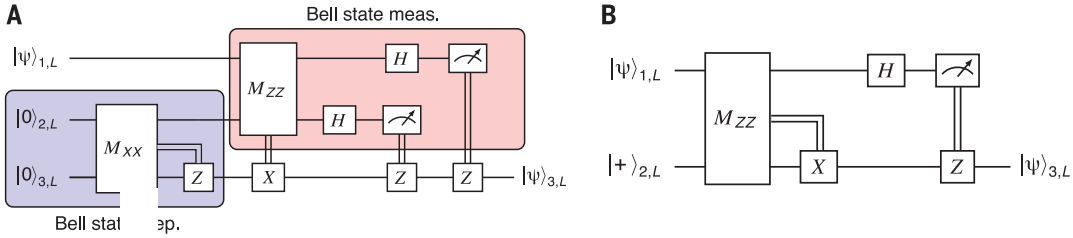

Fig. 4. Two different implementations of logical teleportation circuits using a lattice surgery gate set. The first circuit (**A**) is analogous to the transversal implementation in Fig. 3. The second circuit (**B**) is logically equivalent (see fig. S1) but does not use a Bell resource state and uses fewer logical qubits.

In this work, we partially benchmarked transversal versus lattice surgery gate sets using the teleportation protocol. Although the use of an algorithm to compare gates is indirect, it is problematic to directly compare the different gate sets because they implement different logic, and it is more meaningful to compare different implementations of the same algorithm. As other algorithms will be more efficiently expressed in one versus another gate set, to get a more complete picture, it would be useful to extend these comparisons to additional algorithms or protocols.

To partially understand the better performance of the transversal gate set, we note the presence of additional noise in the $M_{XX}M_{ZZ}$ circuits stemming from two sources: (i) an increased gate count compared with the transversal circuits (a maximum of 260 CNOTs versus a maximum of 158 and 106 CNOTs for 1QEC and 0QEC, respectively) and (ii) an increased number of transport steps leading to more memory error (*9*) (see SM supplementary text section 4).

The fidelities for the 0QEC, 1QEC, and the $M_{XX}M_{ZZ}$ circuits drop according to the number of transport steps and gate count, but M_{ZZ} is an outlier that can partially be understood as a substantial difference in structure. The M_{ZZ} circuit consists of only two logical qubits instead of three; less syndrome information is collected and used, and different resource states are prepared (Bell pair versus $|+\rangle_L$).

Conclusions

In general, the results of this work suggest near-break-even performance for small Clifford circuits. In particular, the process fidelity of the physical teleportation experiment is estimated at 0.9895 ± 3. The 0QEC experiment exhibits a process fidelity of 0.989 ± 2, suggesting a break-even milestone, although a larger statistical separation would be necessary to be conclusive and may require further optimization. Optimization was facilitated by using the SLR programming language (*38*, *39*) for logical circuits (see SM supplementary text section 1). Potential improvements include exploring alternative QEC protocols, reducing leakage errors (*40*–*42*), applying Clifford deformation (*43*–*45*), dynamical decoupling, Pauli twirling, and using larger distance codes (*46*). Enhanced decoding could also be achieved by incorporating biased noise knowledge and decoding all measured syndromes (*8*, *14*, *47*, *48*,).

The results in this work represent the state of the art in experimental QEC; however, more work is needed to demonstrate the error suppression promised by QEC. We believe that fundamental limitations are not an issue. The main noise source in the two-qubit gate is spontaneous emission, which can be mitigated by adjusting laser wavelengths and power (*49*). Memory errors, particularly coherent ones, are a concern for deep logical programs. No effort was made to improve performance beyond optimization of the input program, and results represent performance achievable by external users. Our results were obtained using Quantinuum's H-series compiler, which is general-purpose rather than optimized for error correction. Custom compilation and QCCD ion traps with 2D geometries (*50*) could improve performance and clock speed.

Understanding the trade-off between fault-tolerant implementations of algorithms versus error suppression is crucial as quantum devices scale up. We demonstrate the first logical state teleportation and lattice surgery for a QEC code, showcasing QCCD technology's versatility. Similarly, another trapped-ion processor demonstrated code-switching (*51*), enabling non-Clifford operations suitable for QCCD architectures. This work lays groundwork for the experimental investigation of the fault-tolerant implementation of quantum algorithms through QEC. Expansion of this work may include optimizing resource requirements, including state generation, gate set comparisons, and practical fault tolerance; co-designing quantum hardware; and tailoring QEC protocols to advance large-scale quantum computing.

REFERENCES AND NOTES

1. C. H. Bennett *et al*., *Phys. Rev. Lett.* **70**, 1895–1899 (1993).
2. D. Bouwmeester *et al*., *Nature* **390**, 575–579 (1997).
3. D. Boschi, S. Branca, F. De Martini, L. Hardy, S. Popescu, *Phys. Rev. Lett.* **80**, 1121–1125 (1998).
4. M. Riebe *et al*., *Nature* **429**, 734–737 (2004).
5. M. D. Barrett *et al*., *Nature* **429**, 737–739 (2004).
6. S. Olmschenk *et al*., *Science* **323**, 486–489 (2009).
7. A. Erhard *et al*., *Nature* **589**, 220–224 (2021).
8. D. Bluvstein *et al*., *Nature* **626**, 58–65 (2024).
9. S. A. Moses *et al*., *Phys. Rev. X* **13**, 041052 (2023).
10. M. A. Nielsen, *Phys. Lett. A* **303**, 249–252 (2002).
11. K. Mayer *et al*., arXiv:2404.08616 [quant-ph] (2024).
12. C. Baldwin, Quantinuum Hardware Specifications, GitHub (2022); https://github.com/CQCL/quantinuum-hardware-specifications.
13. P. Aliferis, D. Gottesman, J. Preskill, *Quantum Inf. Comput.* **6**, 97–165 (2006).
14. N. Delfosse, A. Paetznick, arXiv:2304.05943 [quant-ph] (2023).
15. A. M. Steane, *Phys. Rev. Lett.* **77**, 793–797 (1996).
16. D. Nigg *et al*., *Science* **345**, 302–305 (2014).
17. J. Hilder *et al*., *Phys. Rev. X* **12**, 011032 (2022).
18. L. Postler *et al*., *Nature* **605**, 675–680 (2022).
19. C. Ryan-Anderson *et al*., *Phys. Rev. X* **11**, 041058 (2021).
20. C. Ryan-Anderson *et al*., arXiv:2208.01863 [quant-ph] (2022).
21. M. P. da Silva *et al*., arXiv:2404.02280 [quant-ph] (2024).
22. B. W. Reichardt, *Quantum Sci. Technol.* **6**, 015007 (2020).
23. M. A. Nielsen, I. L. Chuang, *Quantum Computation and Quantum Information* (Cambridge Univ. Press, 2000).
24. E. Knill, arXiv:quant-ph/0404104 [quant-ph] (2004).
25. E. Knill, arXiv:quant-ph/0402171 [quant-ph] (2004).
26. E. Knill, *Nature* **434**, 39–44 (2005).
27. P. Aliferis, D. Gottesman, J. Preskill, *Quantum Inf. Comput.* **8**, 181–244 (2008).
28. H. Goto, *Sci. Rep.* **6**, 19578 (2016).
29. E. Knill, arXiv:quant-ph/0312190 [quant-ph] (2004).
30. D. J. Wineland *et al*., *J. Res. Natl. Inst. Stand. Technol.* **103**, 259–328 (1998).
31. A. J. Landahl, C. Ryan-Anderson, arXiv:1407.5103 [quant-ph] (2014).
32. D. Horsman, A. G. Fowler, S. Devitt, R. Van Meter, *New J. Phys.* **14**, 123011 (2012).
33. E. Dennis, A. Kitaev, A. Landahl, J. Preskill, *J. Math. Phys.* **43**, 4452–4505 (2002).
34. T. J. Yoder, I. H. Kim, *Quantum (Vienna)* **1**, 2 (2017).
35. D. Litinski, *Quantum (Vienna)* **3**, 128 (2019).
36. X. Zhou, D. W. Leung, I. L. Chuang, *Phys. Rev. A* **62**, 052316 (2000).
37. H. Poulsen Nautrup, N. Friis, H. J. Briegel, *Nat. Commun.* **8**, 1321 (2017).
38. C. Ryan-Anderson, PECOS: Performance Estimator of Codes On Surfaces, GitHub (2018); https://github.com/PECOS-packages/PECOS.
39. C. Ryan-Anderson, "Quantum algorithms, architecture, and error correction," thesis, University of New Mexico (2018).
40. D. Hayes *et al*., *Phys. Rev. Lett.* **124**, 170501 (2020).
41. M. Suchara, A. W. Cross, J. M. Gambetta, in *2015 IEEE International Symposium on Information Theory (ISIT)* (IEEE, 2015), pp. 1119–1123.
42. N. C. Brown, A. Cross, K. R. Brown, in *2020 IEEE International Conference on Quantum Computing and Engineering (QCE)* (IEEE, 2020), pp. 286–294.
43. D. K. Tuckett, S. D. Bartlett, S. T. Flammia, *Phys. Rev. Lett.* **120**, 050505 (2018).
44. J. P. Bonilla Ataides, D. K. Tuckett, S. D. Bartlett, S. T. Flammia, B. J. Brown, *Nat. Commun.* **12**, 2172 (2021).
45. M. Vasmer, A. Kubica, *PRX Quantum* **3**, 030319 (2022).
46. J. K. Iverson, J. Preskill, *New J. Phys.* **22**, 073066 (2020).
47. D. Bacon, S. T. Flammia, A. W. Harrow, J. Shi, *IEEE Trans. Inf. Theory* **63**, 2464–2479 (2017).
48. D. Gottesman, arXiv:2210.15844 [quant-ph] (2022).
49. R. Ozeri *et al*., *Phys. Rev. A* **75**, 042329 (2007).
50. R. D. Delaney *et al*., arXiv:2403.00756 [quant-ph] (2024).
51. I. Pogorelov *et al*., arXiv:2403.13732 [quant-ph] (2024).

52. C. Ryan-Anderson, Publication data set, GitHub (2024); https://github.com/ciaranra/paper-arxiv-2404-16728.
53. C. Ryan-Anderson, Publication data set, version 0.1.0, Zenodo (2024); https://doi.org/10.5281/zenodo.13138465.

ACKNOWLEDGMENTS

We acknowledge the team at Quantinuum for all their contributions and the fabrication facility at Honeywell for producing world-class ion traps. We also thank B. Criger for helpful discussions, J. Colina for helping develop the H2-1 compiler, and the people at IARPA for inspiring discussions. Lastly, we thank T. Uttley for his leadership and support. **Funding:** The authors declare that all funding was provided internally by Quantinuum. **Author contributions:** C.R.-A. designed the study, gathered the data, and contributed to all code specific to the experiments described in this work, including circuit constructions and data analysis. N.C.B. contributed the visualizations. C.R.-A., N.C.B., and D.H. contributed to writing the original draft as well as further reviewing and editing of the manuscript. C.H.B. and K.M. contributed to the data analysis. J.M.D., C.F., J.P.G., T.M.G., N.H., C.H., C.V.H., J.J., D.L., T.M., M.Ma., Y.M., M.Mi., S.A.M., B.N., J.P., P.S., R.P.S., and J.W. contributed to the construction and maintenance of the H2 device used to collect the data. **Competing interests:** The authors declare that they have no competing interests. **Data and materials availability:** All data are available in the manuscript or the supplementary materials or are deposited in GitHub (*52*). The code for this work is available in Zenodo (*53*).

SUPPLEMENTARY MATERIALS

science.org/doi/10.1126/science.adp6016
Supplementary Text
Figs. S1 to S5
Tables S1 to S14
References (*54*–*61*)

Submitted 2 April 2024; accepted 16 August 2024
10.1126/science.adp6016